REPORT DOCUMENTATION PAGE

Public reporting burden for this collection of information is estimated to average 1 hour per response, including the time for reviewing instructions, searching existing data sources, gathering and maintaining the data needed, and completing and reviewing the collection of information. Send comments regarding this burden estimate or any other aspect of this collection of information, including suggestions for reducing this burden, to Washington Headquarters Services, Directorate for Information Operations and Reports, 1215 Jefferson Davis Highway, Suite 1204, Arlington, VA 22202-4302, and to the Office of Management and Budget, Paperwork Reduction Project (0704-0188), Washington, DC 20503.

1. AGENCY USE ONLY *(Leave blank)*	2. REPORT DATE 21 Sept 99	3. REPORT TYPE AND DATES COVERED Final Report 1 Jul 96 – 30 Jun 99

4. TITLE AND SUBTITLE
Solid-Gas Interface Analyses for High Energy Density Fuels Combustion

5.   FUNDING NUMBERS
G   N00014-96-1-1194

6.   AUTHORS
Corin Segal

7.   PERFORMING ORGANIZATION NAME(S) AND ADDRESS(ES)
University of Florida
Aerospace Engineering, Mechanics & Engineering Science
231 Aerospace Building
Gainesville FL 32611

8. PERFORMING ORGANIZATION REPORT NUMBER

8.   SPONSORING/MONITORING AGENCY NAME(S) AND ADDRESS(ES)
US Department of Navy
Office of Naval Research
800 North Quincy Street
Arlington, VA 22217-5660

10. SPONSORING/MONITORING REPORT NUMBER

19991004 255

11. SUPPLEMENTARY NOTES

12a. DISTRIBUTION/AVAILABILITY STATEMENT

APPROVED FOR PUBLIC RELEASE

12b. DISTRIBUTION CODE

13. ABSTRACT *(Maximum 200 words)*

New hydrocarbon fuels with high energy-density content can substantially advance high-thrust, high-temperature, and reduced-size combustion technology. In the present work, the phase change dynamics of the PCU alkene dimer, a newly synthesized high energy-density hydrocarbon fuel, in turbulent reacting flows has been investigated. The shape, location and velocity of the propellant-gas interface has been treated explicitly. A Lagrangian moving grid technique in conjunction with an established body-fitted field equation solver has been developed. Due to the complex flow structure and uneven heat flux distribution along the propellant surface, the interface experiences nonuniform regression between the front and the rear ends. Consistent with the experimental observation, the thermal characteristics near the solid-gas interface vary in space and in time. The present computational capability can advance our understanding of phase change, thermal decomposition, and subsequent mixing and burning dynamics of energetic fuels.

14. SUBJECT TERMS
Interface modeling , High Energy-Density Fuels, Energetic Compounds

15. NUMBER OF PAGES

16. PRICE CODE

17. SECURITY CLASSIFICATION OF REPORT Unclassified	18. SECURITY CLASSIFICATION OF THIS PAGE Unclassified	19. SECURITY CLASSIFICATION OF ABSTRACT Unclassified	20. LIMITATION OF ABSTRACT UL

NSN 7540-01-280-5500   Computer Generated   STANDARD FORM 298 (Rev 2-89)

DTIC QUALITY INSPECTED 4

ONR Grant N00014-96-1-1194

Final Report

Solid-Gas Interface Analyses for High Energy Density Fuels Combustion

submitted by

Corin Segal

ABSTRACT

New hydrocarbon fuels with high energy-density content can substantially advance high-thrust, high-temperature, and reduced-size combustion technology. In the present work, the phase change dynamics of the PCU alkene dimer, a newly synthesized high energy-density hydrocarbon fuel, in turbulent reacting flows has been investigated. The shape, location and velocity of the propellant-gas interface has been treated explicitly. A Lagrangian moving grid technique in conjunction with an established body-fitted field equation solver has been developed. Due to the complex flow structure and uneven heat flux distribution along the propellant surface, the interface experiences nonuniform regression between the front and the rear ends. Consistent with the experimental observation, the thermal characteristics near the solid-gas interface vary in space and in time. The present computational capability can advance our understanding of phase change, thermal decomposition, and subsequent mixing and burning dynamics of energetic fuels.

NOMENCLATURE

F	interface position
g	gravitational acceleration
J	Jacobian
k	thermal conductivity
L	latent heat of fusion
$\vec{n}$	unit normal vector
q_1, q_2, q_3	metrics of transformation
S	source term
$\vec{t}$	unit tangent vector
T	temperature
(u, v)	Cartesian components of the fluid velocity vector
(U,V)	contravariant velocity components
V_N	front velocity
(x,y)	Cartesian coordinates
$\dot{x}, \dot{y}$	Cartesian components of the grid velocity vector

Greek symbols

ξ, η	curvilinear coordinates
$k-\varepsilon$	turbulent kinetic energy and rate of dissipation
μ	fluid viscosity
ϕ	dependent variable
ϱ	density
τ	time

Subscripts

f fluid

s solid

Superscripts

n   number of time–step

1. Introduction

To continue to improve the performance of air–breathing propulsion systems, much attention has been given to means to increase the energy–density of existing fuels. For example, metallic/nonmetallic materials such as aluminum and boron can be employed in conjunction with either conventional liquid hydrocarbons to form slurries, or other fuels to form dual-base propellants. New hydrocarbon fuels with high energy–density content have also been synthesized and their combustion characteristics assessed under a variety of thermodynamic airflow conditions. Marchand [1], Segal and Shyy [2], and Yang and Zarko [3] have reviewed various aspects of these research activities. In the present work, we discuss recent efforts in advancing our capabilities in predicting and analyzing the combustion characteristics of PCU alkene dimer [4], a newly synthesized high energy-density hydrocarbon fuel. This propellant offers much promise to substantially contribute to high–thrust, high–temperature, and reduced-size combustion technology. However, since it has been synthesized only recently, much research and development efforts, both experimentally and theoretically, will be required before it can be applied to practical systems.

For the present and many other solid energetic materials, key physical processes, including melting/evaporation, pyrolysis, and mixing and combustion, can have different time scales, causing concerns regarding ignition and efficiency of the combustion process. To facilitate phase change, a high temperature gas stream is usually introduced to melt and evaporate the condensed fuel, often creating complex flow structures [5, 6]. In many cases, the solid fuel melts first before being

3

evaporated and going through the pyrolysis process. However, in the present work, only solid and gas phases are considered, which, under the combustion condition, is a reasonable approximation.

Fundamentally, phase change characteristics are dictated by the rate and distribution of the excess heat flux into the condensed fuel from the high temperature environment in order to fulfill the latent heat requirement. Accordingly, for sustained burning, the shape and the rate of the movement of the phase boundary change in time. These aspects need to be determined as a part of solutions to the fluid dynamics and combustion processes. Computationally, the existence of the moving phase boundary creates a major difficulty since the locations and physical parameters governing motion of the phase boundary, such as heat flux, species concentration, and interface velocity vary from location to location, and are not known *a priori* [7]. Much literature exists in treating the multiphase flow phenomena; for summary and references to computational modeling issues, see Refs. [7, 8].

The pyrolysis process, including thermal decomposition and chemical reaction to form intermediate species prior to combustion, closely interacts with the phase change process. In particular, the unsteadiness of the phase change process and mixing between the evaporated energetic fuel and surrounding gas stream are of major importance to effective combustion. In many models, the phase change and pyrolysis processes are not only lumped together but also treated as a surface phenomenon. With the lumped surface treatment, the condensed phase reaction layer and the gas phase region are often considered to be capable of responding instantaneously to changing external conditions such as the combusting gas stream, allowing a quasi-steady model to be employed. Furthermore, for both energy and species transport aspects, the effects of chemical reaction appear only through boundary conditions between the non-reacting condensed phase and the gas phase, e.g., Ref. [9]. While this type of model reduces the computational complexities substantially, it has been found inadequate in capturing the physical mechanisms involved [10]. A less restrictive model can be derived based on the notion of distributed condensed phase reaction [6, 10] where both energy and species transport equations need to be solved. In these models, however, the aforementioned phase change process is often drastically simplified or neglected.

4

In addition to phase change and pyrolysis, mixing between fuel and oxidizer by turbulent motion and molecular diffusion are required in order to sustain continuous combustion. Turbulence and chemistry interaction is a key issue in virtually all practical combustion processes. The modeling and computational issues involved in these aspects have been well exposed in the literature[7, 11–13]. An important factor in the selection of sub–models is "computational tractability", which means that the differential or other equations needed to describe a sub–model should not be so computationally intensive as to preclude their practical application in three-dimensional Navier–Stokes calculations. In virtually all practical flowfield calculations, engineering approximations are required to make the computation tractable.

In the present effort, the issue of tracking the phase change dynamics of the solid energetic fuel in turbulent reacting flows is investigated. The main issue is handling of the moving boundary resulting from evaporation of the solid fuel. In particular, the shape, location and velocity of the propellant interface is treated explicitly. In the following, we will first summarize the salient issues of computing the moving boundary in the context of recirculating, turbulent reacting flows. Then, a methodology will be presented with examples to illustrate the main features of the numerical techniques.

2. Numerical Algorithm

(i) Physical Model and Field Equations Solver

The approach taken here attempts to strike a reasonable balance in handling two competing aspects of the modelling work, namely, the complicated physical and chemical interactions in the flowfield, and the requirements in resolving the multi-dimensional geometrical constraints of the flow field. The key elements of the numerical algorithm and turbulent combustion models embodied in the present effort are: (i) conserved scalar (with assumed pdf to account for variance effect) and fast chemistry approach for turbulence/chemistry interaction [11, 13], (ii) the k–ε two-equation model with wall function treatment for turbulence effects [14], (iii) Semi–implicit iterative

5

algorithm solving strong conservation form of transport equations (mass, momentum, and scalar fields) in general non-orthogonal curvilinear coordinates [7], (iv) second–order finite difference operators for all terms including convection, pressure and diffusion effects [7, 13], and (v) multi-step predictor-corrector method for the pressure correction equation [7]. These elements have been applied to compute many single-phase turbulent reacting flow problems, and have been extensively documented in the literature [7, 13]. The main interest of the present effort is the incorporation of the moving boundary technique into the above solution algorithm.

To illustrate the current approach, the continuity and momentum equations in generalized, nonorthogonal, curvilinear coordinates are presented in the following. The continuity equation, (1a) in nonorthogonal coordinates, $[\xi = \xi(x, y, t), \eta = \eta(x, y, t)]$, can be expressed as,

$$\frac{\partial}{\partial t}(J\rho) + \frac{\partial(\rho U)}{\partial \xi} + \frac{\partial(\rho V)}{\partial \eta} = 0 \qquad (1a)$$

where ρ is density, and

$$J = x_\xi y_\eta - x_\eta y_\xi \qquad (1b)$$

is the Jacobian of the transformation and

$$U = (u - \dot{x}) \, y_\eta - (v - \dot{y}) \, x_\eta$$
$$V = (v - \dot{y}) \, x_\xi - (u - \dot{x}) \, y_\xi \qquad (1c)$$

are the contravariant velocity components. In Eq. (1c), u and v, and $\dot{x}$ and $\dot{y}$ are, respectively, the Cartesian components of the fluid and the grid velocity vector. The momentum equations are

$$\frac{\partial(J\rho u)}{\partial t} + \frac{\partial(\rho U u)}{\partial \xi} + \frac{\partial(\rho V u)}{\partial \eta} = -\left\{ y_\eta \frac{\partial p}{\partial \xi} - y_\xi \frac{\partial p}{\partial \eta} \right\} + \frac{\partial}{\partial \xi}\left[\frac{\mu}{J}\left(q_1 u_\xi - q_2 u_\eta \right) \right]$$
$$+ \frac{\partial}{\partial \eta}\left[\frac{\mu}{J}\left(q_2 u_\xi - q_3 u_\eta \right) \right] + S_u(\xi, \eta) \cdot J \qquad (2a)$$

$$\frac{\partial(J\rho v)}{\partial t} + \frac{\partial(\rho U v)}{\partial \xi} + \frac{\partial(\rho V v)}{\partial \eta} = -\left\{ x_\xi \frac{\partial p}{\partial \eta} - x_\eta \frac{\partial p}{\partial \xi} \right\} + \frac{\partial}{\partial \xi}\left[\frac{\mu}{J}\left(q_1 v_\xi - q_2 v_\eta \right) \right]$$
$$+ \frac{\partial}{\partial \eta}\left[\frac{\mu}{J}\left(q_2 v_\xi - q_3 v_\eta \right) \right] - \left(\rho - \rho_{ref} \right) g \cdot J + S_v(\xi, \eta) \cdot J \qquad (2b)$$

along x and y directions respectively, where x_η, y_η, and so on are the metrics of the transformation and q_1, q_2 and q_3 are defined as

$$q_1 = x_\eta^2 + y_\eta^2$$
$$q_2 = x_\xi x_\eta + y_\xi y_\eta \tag{3}$$
$$q_3 = x_\xi^2 + y_\xi^2$$

Other scalar transport equations, including the k–ε two–equation model [14] and the mean and variance of the conserved scalar employed in the combustion model [13] can be expressed in a similar manner and will not be presented here.

(ii) Boundary Conditions and Interface Tracking Procedure

The boundary conditions on the interface are:

no-slip:

$$\vec{u} \cdot \vec{t} = 0 \tag{4a}$$

mass conservation:

$$\rho_f \vec{u} \cdot \vec{n} = (\rho_s - \rho_f) V_N \tag{4b}$$

where V_N is the normal velocity of the interface, given by the Stefan condition:

$$\rho_s L V_N = \left(k_s \frac{\partial T_s}{\partial n} - k_f \frac{\partial T_f}{\partial n} \right) \tag{4c}$$

Here subscripts f and s stand for fluid and solid, respectively. Additional conditions are applied at the boundaries of the computational domain, where the wall function approach is adopted for the turbulence model.

Several techniques exist for tracking arbitrarily shaped interfaces, each with its own strengths and weaknesses, as summarized by Shyy et al. [8]. These techniques may be classified under two main

categories, namely, Lagrangian methods and Eulerian methods . The main features of the two types are presented in Fig. 1.

In the Lagrangian methods, the grid is configured to conform to the shape of the interface, and thus it adapts continually to it. The Eulerian methods usually employ a fixed grid formulation, and the interface between the two phases is not explicitly tracked but is reconstructed from the properties of appropriate field variables, such as fluid fractions. Based on these basic differences in approach of the two classes of methods, the following comparisons can be made.

1. Interface Definition

The Lagrangian methods maintain the interface as a discontinuity and explicitly track its evolution. If detailed information regarding the interface location is desired, Eulerian methods may need elaborate procedures to deduce the interface location based on the volume fraction information, and uncertainty corresponding to one grid cell is unavoidable. In the Lagrangian case, the interface can be tracked as an $(n-1)$-dimensional entity for an n-dimensional space. No modeling is necessary to define the interface or its effect on the flow field. In the case of Eulerian schemes, modelling or the solution of additional equations is required to obtain information regarding fluid fractions or other functions yielding information in the two-phase regions.

2. Interfacial Boundary Conditions

In the Lagrangian methods, boundary conditions can be applied at the exact location of the interface since the interface position is explicitly known at each instant. In the Eulerian methods, the boundary conditions are manipulated to appear in the governing transport equations. This leads to smearing of boundary information.

3. Discretization of the Domain

In the Lagrangian methods, the grid adapts to the interface and hence grid rearrangement and motion terms have to be incorporated. When the interface begins to distort, the grid needs to be regenerated each time, which may require the solution of another equation. The resulting grid on which the field variables are computed may be skewed and unevenly distributed, thus influencing the accuracy of the field solver. The Eulerian methods have an advantage in this regard since the computations are

performed on a fixed grid, hence obviating the need for grid rearrangement. However, when the interface is arbitrarily shaped, improved resolution in desired regions is difficult to obtain, unless complicated local refinements are adopted.

4. Topological Changes of the Interface

Lagrangian methods have so far experienced difficulty in handling topological changes, mainly due to the breakdown of the structured grid arrangement and the need for redistribution of field information in the vicinity of the interface for unstructured grid methods. On the other hand, in Eulerian methods mergers and fragmentations are taken care of automatically, merely by updating the values of the fluid fraction field. However, the detailed physical features involved during such events may not be fully resolved due to the smearing of information as mentioned above.

Whether a Lagrangian or Eulerian approach is adopted is dependent on the physical problem under investigation. If details of the interface are secondary or are unlikely to significantly impact the global flow features, the Eulerian methods are more attractive. If the discontinuity across the interface is to be maintained with fidelity, and if interfacial behavior is the focus, Lagrangian methods hold an advantage. In the present effort, the Lagrangian approach is well suited because the interface shape in most cases is expected to be tractable by a single–block curvilinear grid system. Furthermore, much experience has been gained over the last decade in employing the body–fitted curvilinear grid to handle the high Reynolds number turbulent reacting flows. More research is required to apply the fixed, Cartesian grid approach, with the cut–cell treatment [8], to turbulent flows.

In developing the Lagrangian approach, definition of the interface shape and estimation of the interface velocity are critical. In both aspects, a key step is to calculate the local normal to the interface. In Eq. (4c) the local normal to the interface is given by

$$\vec{n} = \frac{1}{|\nabla F|} \left(\frac{\partial F}{\partial x} \vec{i} + \frac{\partial F}{\partial y} \vec{j} \right) \tag{5}$$

9

where $F=F(x, y, t)$ is the curve defining the interface. The interface shape is defined in a piecewise fashion to facilitate handling of branched interfaces. Here, as discussed in Ref. [8], a quadratic polynomial fit is performed for three successive nodal points at each point of the interface. Thus, at the ith point on the interface we designate the curve $y_i = a_i x_i^2 + b_i x_i + c_i$, i.e., $F_i = y_i - (a_i x_i^2 + b_i x_i + c_i)$ defines the interface. The a_i, b_i, and c_i are determined from the known values of (x_j, y_j), $j = i-1,..., i+1$.

The quantities F_x and F_y, of course, are directly available in the physical domain from the curve fit. Thus, the new coordinates of the interfacial points are obtained from:

$$x^{n+1} = x^n + \frac{\partial F}{\partial x} \frac{v_n}{|\nabla F|} \delta\tau \tag{6a}$$

$$y^{n+1} = y^n + \frac{\partial F}{\partial y} \frac{v_n}{|\nabla F|} \delta\tau \tag{6b}$$

where $\delta\tau$ is the time step size. Now that these new coordinates of the curve have been determined, an appropriate body–fitted grid system is generated, the flow field is solved for, the curve fit is performed at the interface, and a fresh interface position is obtained from Eqs. (6a and b). All these procedures should be performed in a fully coupled manner involving interaction among the velocity, pressure, temperature, and other scalar variable fields, interface motion, and grid movement at each iteration. In the present study, the main focus is on development of the moving boundary tracking technique, namely, the solid material only experiences phase change but makes no contributions to combustion. However, because the boundary shape changes in time, the flow field responds to the phase change process directly as well.

3. Results and Discussion

The combustion characteristics of the solid fuel are studied by placing it in a rectangular duct; the side view of the initial configuration is illustrated in Fig. 2. Due to the difficulty in igniting the

high–density fuel, a Hydrogen–air flame is employed to provide a pilot flame for ignition of the fuel which is placed downstream as shown in Fig. 3 (a). In the present configuration, inlet velocity of air at left of the chamber was given to be 103 m/s. Hydrogen was injected through the injection orifice at 800 m/s. Both gases are initially at a temperature of 300K. All computations are conducted on 125 x 41 grid, generated to fit the time varying geometry caused by the receding solid propellant interface. The computation is handled by assuming instantaneous establishment of the reacting gas flow field, followed by the phase change simulation. At the end of each time increment, a new solid–gas interface is established, the geometry is redefined, and body–fitted grid regenerated. Based on the new grid, the field equations of mass continuity, momentum, and combustion and turbulence closure models are solved, and new solution obtained. In the present effort, the fluid flow is handled as a quasi–steady problem with incrementally updated boundary shape and location.

The established velocity, temperature and eddy thermal conductivity fields before initiating the phase change simulation are shown in Figs. 3 (a–c). Because of the substantial hydrogen jet momentum and mass fluxes, there is a substantial interaction between it and the main inflow, as evidenced by the blockage effects, curved jet trajectory, and recirculating flow pattern just downstream of the jet. The maximum temperature observed is around 2200K, the adiabatic flame temperature of the H_2–Air mixture. In responding to the convection characteristics, there is less thermal impact on the front portion than on the rear portion of the solid propellant. The eddy thermal conductivity in the region above the solid propellant also exhibits noticeable nonuniformity in magnitude. The combination of the eddy thermal conductivity and temperature distribution dictates the movement of the solid–gas interface.

Figure 4 presents the shape and location of the solid–gas interface at selected time instants. Due to the uneven heat flux distribution along the surface, the interface shape changes in time. For example, the rear portion of the propellant is consumed faster than the front portion. There are also non–smooth spots developed at various time instants, reflecting locally concentrated heat flux. The heat flux distributions at time 0 and 12.5 s are compared in Fig. 5. Clearly, substantial differences in the heat flux distribution exist at different time instants, due to the interaction between the moving

boundary and the turbulent reacting flow. In Fig. 6, the flow configuration and velocity and temperature distributions at the time instant of 12.5 second are depicted. Even though the flow is subsonic, due to the high Reynolds number, the flow structure in the region upstream of the solid propellant is affected little by the time–dependent boundary shape due to phase change. However, the thermal characteristics near the propellant interface show clear sign of time dependency, indicating that the mass flux of the energetic fuel into the hot gas stream varies in time and in space. Consequently, the gas temperature inside the combustor will also vary in time.

Experimentally, average burning rates have been measured using thin wire thermocouples imbedded in the sample at the mid–point and at the three–quarter point from the leading edge of the solid fuel. At each location, the thermocouples are placed at half thickness of the sample. Due to the low thermal conductivity of the fuel, the sample temperature remains nearly constant during combustion, until the fuel burns away at the location of the probes and the rapid temperature increase indicates the surface regression to the known depth. For PCU alkene dimers, at the flow condition investigated here, experimental information indicates that the burning rates at these two locations are 0.336 mm/s and 0.505 mm/s, respectively. Figure 7 shows the experimentally derived surface regression approximated by data at three points: the leading edge of the sample, which remains unburned until the final stages of the sample consumption, and the average burning rates measured at the mid–point and at the three–quarter point. Because only three data points are available, a second–order polynomial is chosen to describe the interface shape, which results in a smoother appearance than actually observed. In contrast, the computational results show substantially more noticeable interface distortion due to uneven heat flux distributions. The surfaces are shown for the same time steps selected in the computation, i.e., from the initial application of the external heat source in 2.5 sec. intervals. Both computational and experimental results show that the consumption of the sample propagates upstream from the recirculation region formed at the trailing edge. Obviously, due to the increased residence time and turbulent mixing in this region, the heat transfer from the burning region to the sample is more intense on the backface of the solid fuel resulting in an accelerated surface regression in this area. In comparison, the leading edge of the sample remains

practically unaffected until the final stages of the sample consumption. It can be seen from the comparison with the calculated data that the experimental results indicate a faster consumption of the fuel sample. This is due to the heat contributed by the fuel itself which is unaccounted for in the present computation. This contribution is quite substantial, especially toward the later stage of the computation because of the accumulation of the PCU alkene dimer in the gas phase. As a result, during the experiment the surface of the sample becomes increasingly distorted towards the trailing edge. Nevertheless, the qualitative agreement between the computational and experimental information offers insight into the predictive capabilities of the present computational model.

4. Concluding Remarks

In the present study, numerical techniques capable of explicitly tracking the receding solid propellant boundary in turbulent reacting flows are developed. With this capability, nonuniform and time dependent heat fluxes along the propellant interface can be predicted, and a two-way coupling between gas-phase and solid-phase is established. A number of areas requiring further efforts can be identified. Clearly, to design high performance combustor using energetic propellants, detailed aspects of the pyrolysis, mixing, and combustion processes need to be better understood. Since the phase change process dictates the supply of the amount of fuel at different times and locations, aspects such as latent heat absorption and subsequent modifications of the interface shape need to be accounted for in presence of these mechanisms. The unsteady interaction between moving phase boundary and chemical kinetics, in both pyrolysis and burning stages, will be investigated using the capability developed in the present effort.

5. Acknowledgment

6. References

1. A.P. Marchand, Polycyclic Cage Compounds: Reagents, Substrates and Materials for the 21st Century, *Aldrichchimica Acta*, Vol. 28, pp. 95–104, 1995.

2. C. Segal and W. Shyy, Energetic Fuels for Combustion Applications, *ASME Journal Energy Resources Technology*, Vol. 118, pp. 180–186, 1996.

3. V. Yang. and V.E. Zarko, Special Issue of *Journal of Propulsion and Power*, Vol. 11, No. 4, 1995.

4. C. Segal, M.J. Friedauer, H.S. Udaykumar, W. Shyy and A.P. Marchand, Ignition Characteristics of a High–Energy Density Fuel in High Speed Flows, to be published in *Journal of Propulsion and Power.*

5. N. Lupoglazoff. and E. Vuillot, Parietal Vortex Shedding as a Cause of Instability for Long Solid Propellant Motors – Numerical Simulations and Comparisons with Firing Tests, *AIAA Paper No. 96–0761,* 1996.

6. Y.–C. Liau and V. Yang, Analysis of RDX Monopropellant Combustion with Two–Phase Surface Reactions, *Journal of Propulsion and Power*, Vol. 11, pp.729–739, 1995.

7. W. Shyy, *Computational Modeling for Fluid Flow and Interfacial Transport*, Elsevier, 1994.

8. W. Shyy, H.S. Udaykumar, M.M.Rao, and R.W. Smith, *Computational Fluid Dynamics with Moving Boundaries*, Taylor & Francis, 1996.

9. N. Zhou and A. Krishnan, A Numerical Model for Endothermic Fuel Flows with Heterogeneous Catalysis, *AIAA Paper No. 96–0650, 1996.*

10. M.Q. Brewster, M.A. Zebrowski, T.B. Schroeder, and S.F. Son, Unsteady Combustion Modeling of Energetic Fuels, *AIAA Paper No. 95–2859,* 1995.

11. P.A. Libby and F.A. Williams, (eds.), *Turbulent Reacting Flows*, Academic Press, 1994.

12. E.S. Oran and J.P. Boris, J.P., *Numerical Simulation of Reactive Flow,* Elsevier, 1987.

13. S.M. Correa and W. Shyy, Computational Models and Methods for Continuous Gaseous Turbulent Combustion, *Progress in Energy and Combustion Science*, Vol. 13, pp.249–292, 1987.

14. B.E. Launder and D.B. Spalding, The Numerical Computation of Turbulent Flow, *Computer Methods in Applied Mecahnics and Engineering*, Vol. 3, pp. 269–289, 1974.
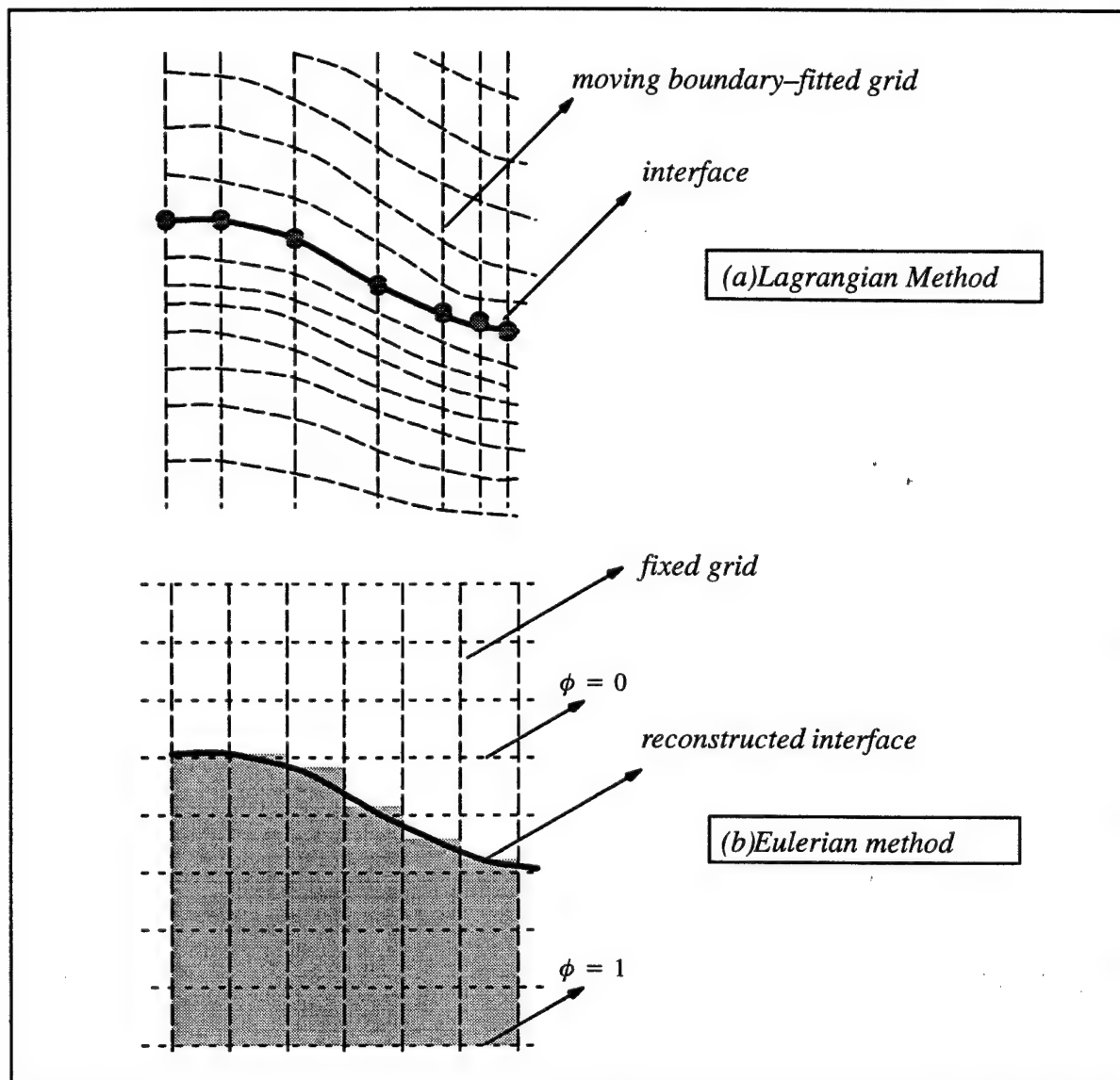
Figure 1. Comparison of Lagrangian and Eulerian methods for interface tracking. (a) Purely Lagrangian method with a moving, boundary conforming grid. (b) Fixed grid Eulerian method with a phase fraction definition of the interface.
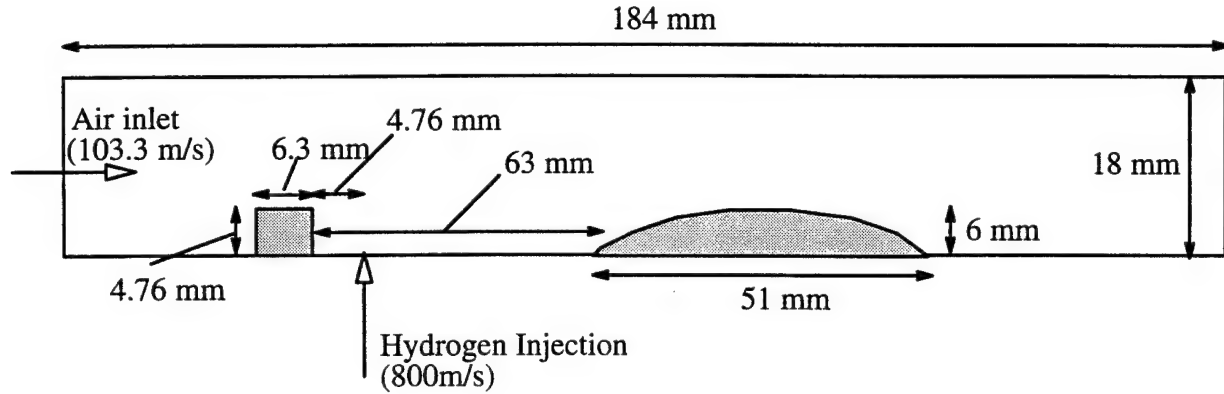
Figure 2. Schematic of the geometrical configuration for hydrogen–air flame and propellant burning. The geometry was chosen to correspond to the experimental setup. The propellant was initially assigned as a circular arc segment as shown above. The relevant material properties: density of air=1.91 kg/m³ and hydrogen=0.0898 kg/m³. For the turbulent quantities: at the inlet $k=(0.03U_{inlet})^2 = 9.59 \ (m/s)^2$, $\varepsilon= (C_\mu k^{3/2}/0.03L_{inlet}) = 6360 \ m^2/s^3$, $\mu_t= C_\mu \varrho k^2/\varepsilon = 0.00248$ kg/ms. For the fuel sample, melting point of fuel sample=450K, latent heat of fuel=72.7 J/g.

(a)

(b)

1– 990 K , 2– 1830 K , 3– 720 K , 4– 2150K , 5– 1550K

(c)

1– 1.5 W/mK, 2– 8.9 W/mK , 3– 1.8 W/mK, 4– 6.1 W/mK, 5– 1.0 W/mK, 6–
3.2 W/mK, 7– 7.1 W/mK , 8– 4.3 W/mK, 9– 2.0 W/mK
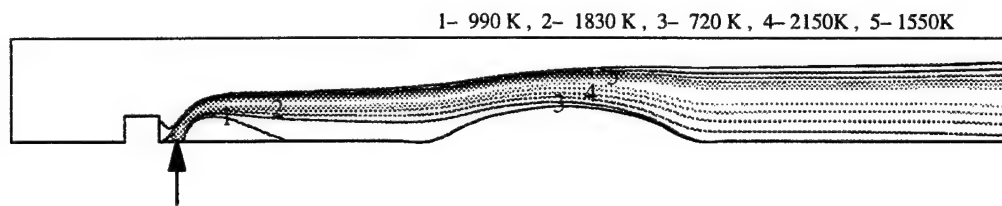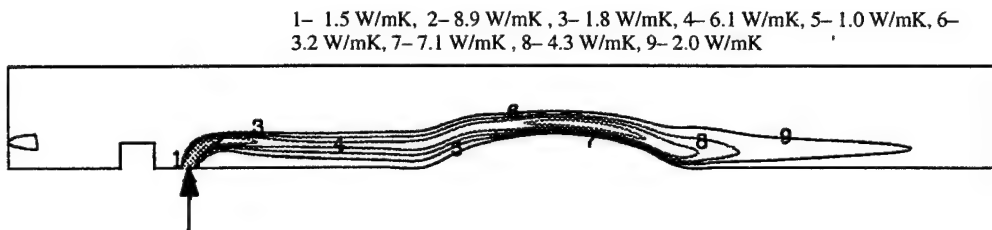
Figure 3. The flow characteristics at t=0, i.e. before propellant regression is
initiated. The hydrogen injection location is indicated by the arrow.
(a) Streamlines at the initial stage. The recirculations due to the step and
behind the jet allow for better mixing of the fuel and air. (b) Isotherms
showing the location of the hydrogen–air flame. The values corresponding
to the numbered contours are indicated. (c) Eddy thermal conductivity con-
tours.
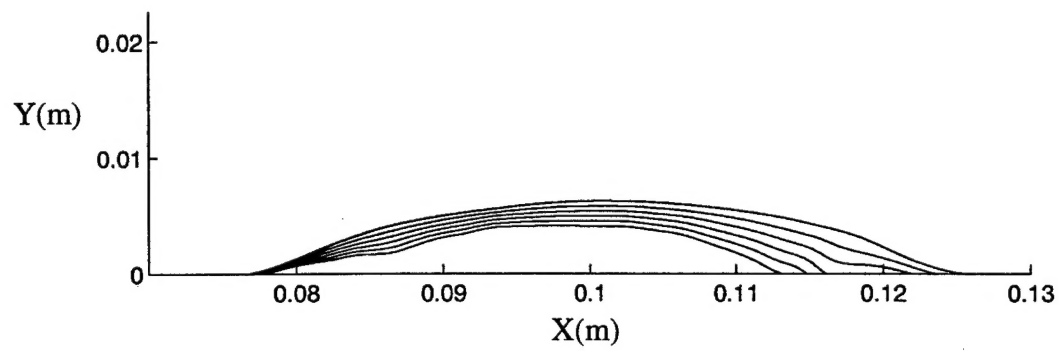
Figure 4. Computed shape of the propellant–gas interface at selected time instants. Curves from top to bottom correspond to t=0.0, 2.5, 5.0, 7.5, 10.0 and 12.5 seconds.

(a)

(b)
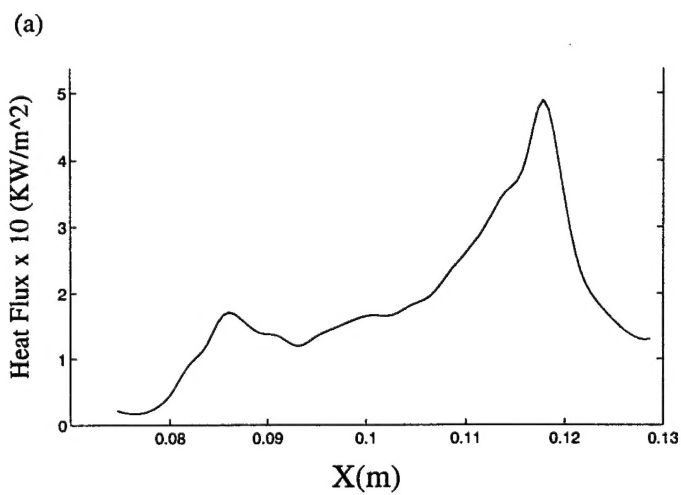
Figure 5. Heat flux distribution
on the interface between pro-
pellant and gas. The heat flux is
shown as a function of the x–
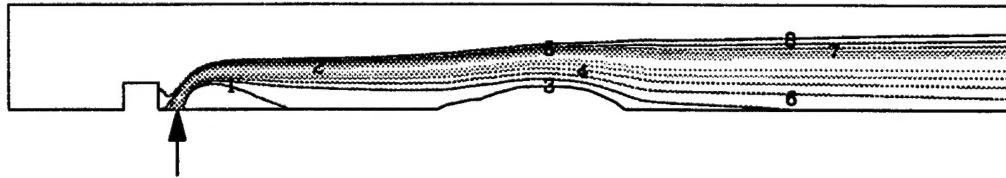coordinate at (a) t=0 and (b)
t=12.5 seconds.

(a)

(b)
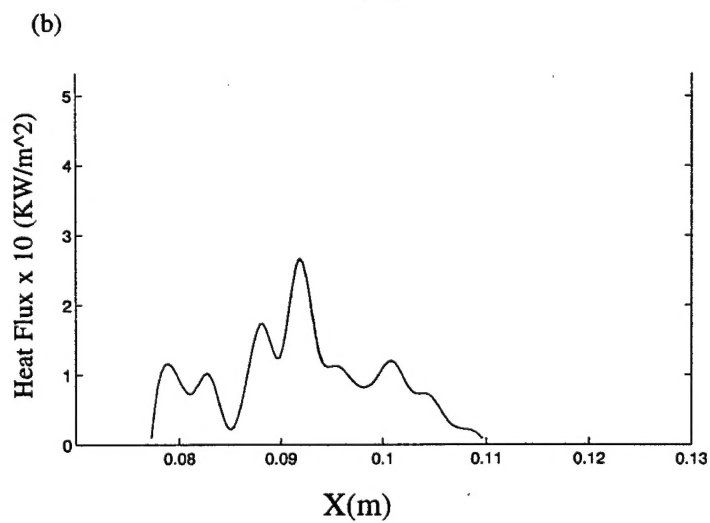
1– 990 K , 2– 1830 K , 3– 720 K , 4– 2150K , 5– 1550K, 6– 1150K, 7–
1160K, 8– 1620 K

(c)

1– 1.5 W/mK, 2– 9.0 W/mK , 3– 1.8 W/mK, 4– 6.1 W/mK, 5– 1.9 W/mK, 6–
3.2 W/mK, 7– 7.3 W/mK , 8– 4.1 W/mK, 9– 2.3 W/mK

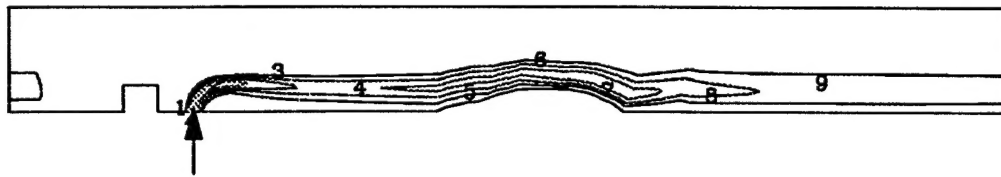*Figure 6. The flow characteristics at t=12.5. The hydrogen injection location is indicated by the arrow. The regressed shape of the bump is shown clearly in Figure 4 at this instant. (a) Streamlines at the initial stage. The recirculations due to the step and behind the jet allow for better mixing of the fuel and air. (b) Isotherms showing the location of the hydrogen–air flame. The values corresponding to the numbered contours are indicated. The isotherms are shown to be lifted away from the solid–gas interface in contrast to Figure 3, thus leading to the lower heat flux values in Figure 5(b). (c) Eddy thermal conductivity contours.*
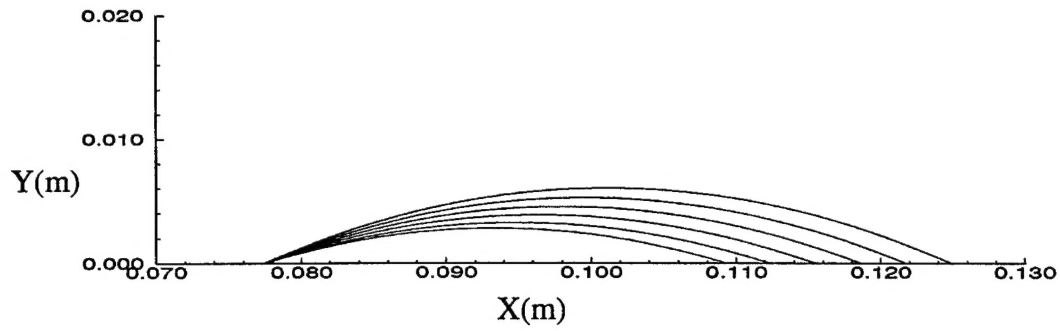
Figure 7. Experimentally estimated shape of the propellant–gas interface at selected time instants. Curves from top to bottom, corresponding to t=0.0, 2.5, 5.0, 7.5, 10.0 and 12.5 seconds, are constructed based on information at three locations.